PHYSICAL REVIEW FLUIDS **5**, 024302 (2020)

Editors' Suggestion

Friction scaling laws for transport in active turbulence

Sanjay C. P. and Ashwin Joy*

Department of Physics, Indian Institute of Technology Madras, Chennai-600036, India

(Received 29 May 2019; revised manuscript received 5 October 2019; accepted 28 January 2020; published 13 February 2020)

Understanding the role of frictional drag in diffusive transport is an important problem in the field of active turbulence. Using a generic continuum model that applies well to living systems, we investigate the role of Ekman friction on the passive transport of Lagrangian tracers that go with the local flow. We find that the crossover from ballistic to diffusive regime happens at a timescale τ_c that attains a minimum at zero friction, meaning that both injection and dissipation of energy delay the relaxation of tracers. We explain this by proposing that $\tau_c \sim \ell^*/u_{\rm rms}$, where ℓ^* is a dominant length scale extracted from energy spectrum peak, and $u_{\rm rms}$ is a velocity scale that sets the kinetic energy at steady state; both scales monotonically decrease with friction. Finally, we predict friction scaling laws for ℓ^*, $u_{\rm rms}$, and the diffusion coefficient $\mathcal{D} \sim \ell^* u_{\rm rms}/2$, that are valid over a wide range of fluid friction. The findings of our report should apply to transport phenomena in generic active systems such as dense bacterial suspensions, microtubule networks, or even artificial swimmers, to name a few.

DOI: 10.1103/PhysRevFluids.5.024302

I. INTRODUCTION

From a cup of coffee to the scales of the interstellar medium, fluid turbulence is ubiquitous in nature [1,2]. Often stated as the last unsolved problem of classical physics, turbulence is actually an ensemble of nonlinear processes that usually happens in any fluid which is far from equilibrium. These nonlinear processes are responsible for cascading the fluid energy throughout the inertial range of wave numbers, i.e., between the scale of injection where turbulence is excited to the scale of damping where viscosity plays a dominant role [3,4]. The large number of degrees of freedom that are coupled by these nonlinear processes display highly irregular dynamics and impose a pressing need for a statistical treatment of turbulence. A natural concern is whether the statistical predictions made in the inertial range are universally applicable; for instance, will the predicted scaling laws hold for general patterns of energy injection, transfer, and dissipation? Relevant scenarios include mesoscale turbulence in active fluids such as bacterial suspensions, microtubule networks, or even artificial swimmers [5–8]. It is therefore very interesting to see whether established results of classical turbulence can be extended to these active fluids. One problem that naturally forms a basis for a statistical treatment of turbulence is the transport of passive tracers advected by the local Eulerian flow. In this paper, we report a detailed study of transport in a distribution of such passive tracers in a two-dimensional (2D) active fluid that describes dense bacterial suspensions well. We record the mean-squared displacements mean square displacement (MSD) of these passive tracers and find that the crossover time from ballistic regime to diffusive regime has a minimum when the fluid friction is zero. The other two cases, namely, positive friction (energy damping) and negative friction (energy injection), both tend to progressively increase the crossover time. We

*ashwin@iitm.ac.in

explain this minimum in crossover time by directly invoking appropriate scaling arguments in the homogeneous steady state of the turbulent fluid. Finally, we set up a universal friction scaling law for the diffusion coefficient of these passive tracers that is in excellent agreement with our direct numerical simulations. Below we provide the organization of our paper.

The presentation of work is organized as follows: In Sec. II, we describe the continuum model and the numerical methods employed to solve the equations; Sec. III goes through the theoretical predictions and numerical verification of our results. We propose a possible experimental realization of our numerical simulations in Sec. IV and conclude in Sec. V by discussing the significance of our work and future directions.

II. CONTINUUM MODEL/NUMERICAL METHODS

The literature on continuum theories of active matter with particular emphasis on collective behavior, is quite extensive [9–16]. In our work, we use a minimal phenomenological model that was recently developed to study turbulence in a dense suspension of bacterium, *Bacillus subtilis* [17–22]. According to this model, at high enough concentration, this bacterial suspension can be approximated as an incompressible fluid, whose velocity field is governed by the following equations:

$$\frac{\partial \boldsymbol{u}}{\partial t} + \lambda_0(\boldsymbol{u}\cdot\nabla)\boldsymbol{u} = -\nabla P - \Gamma_0\nabla^2\boldsymbol{u} - \Gamma_2\nabla^4\boldsymbol{u} - \mu(u)\boldsymbol{u},$$
$$\nabla\cdot\boldsymbol{u} = 0, \tag{1}$$

where P is pressure and the coefficient of the advective term λ_0 decides the type of bacteria, meaning it is either a *pusher* or a *puller*, corresponding to the case $\lambda_0 > 0$ or $\lambda_0 < 0$, respectively. The model also provides internal drive/dissipation through the terms $\Gamma_{0,2}$ and the scalar field $\mu(u) = \alpha + \beta|\boldsymbol{u}|^2$, introduced by Toner and Tu to model the "flocking" behavior in self-propelled rodlike objects [23–25]. Keeping $\Gamma_{0,2} > 0$ leads to destabilization of a band of wave vectors that mimics energy injection into the bacterial suspension mediated by fluid instabilities. While the parameter α, hereafter referred to as the Ekman friction, can produce the effect of energy damping ($\alpha > 0$) as well as energy injection ($\alpha < 0$), the parameter β, however, is restricted to have only positive values and is taken to be 0.5 throughout our paper to remain consistent with earlier works. In order to nondimensionalize Eq. (1), we normalize all distances to $l_0 = 5\pi/k_0$, where $k_0 = \sqrt{\Gamma_0/(2\Gamma_2)}$ is the fastest growing mode in the linear regime characterized by the growth rate: $\gamma(k) = -\alpha + \Gamma_0 k^2 - \Gamma_2 k^4$ [19]. Further defining a characteristic velocity unit, $u_0 = \sqrt{\Gamma_0^3/\Gamma_2}$, one obtains the normalization for time as $t_0 = l_0/u_0$. In these units, we set the values of $\Gamma_0 = (5\pi\sqrt{2})^{-1}$, $\Gamma_2 = (5\pi\sqrt{2})^{-3}$, and $\lambda_0 = 3.5$ to remain consistent with earlier works [17,19]. All physical quantities henceforth appearing in this paper are expressed in these reduced units. Since we are dealing with 2D incompressible flows, it is natural to work in vorticity-stream-function formulation where the governing equations (1) effectively become a single scalar equation. To this end, we rewrite Eqs. (1) as

$$\frac{\partial \boldsymbol{\omega}}{\partial t} + \lambda_0(\boldsymbol{u}\cdot\nabla)\boldsymbol{\omega} = -\Gamma_0\nabla^2\boldsymbol{\omega} - \Gamma_2\nabla^4\boldsymbol{\omega} - \mu(u)\boldsymbol{\omega}, \tag{2}$$

where $\boldsymbol{\omega} = \nabla\times u$ is the vorticity field associated with the flow. Equation (2) is numerically solved using a pseudospectral approach [26] on a grid of 512^2 points over a periodic square box of size 2π. Starting from random vortices, Eq. (2) is evolved in time using the Crank-Nicholson scheme with a time step $\Delta t = 2\times10^{-4}$. Numerical stability is guaranteed by satisfying the Courant-Friedrichs-Lewy criterion, $(u_x/\Delta_x + u_y/\Delta_y)\Delta t \leqslant 1$, where $u_{x,y}$ and $\Delta_{x,y}$ are, respectively, the components of the velocity field and grid spacing in two dimensions. Transport properties are further studied by adding $N = 10\,000$ tracer particles that are advected by the local bacterial flow, and with the dynamics

$$\frac{d\boldsymbol{x}_i(t)}{dt} = \boldsymbol{u}(\boldsymbol{x}_i(t), t), \tag{3}$$

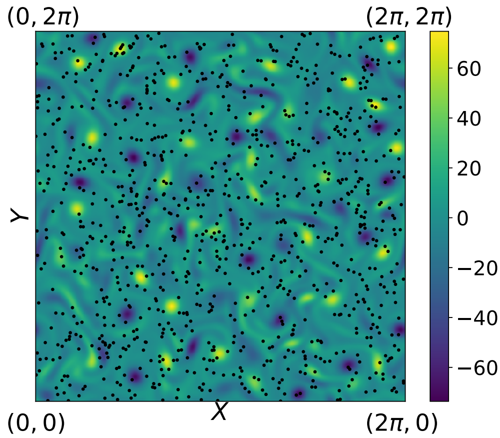

FIG. 1. Color map of the 2D vorticity field along with the distribution of passive tracers, which are indicated as black dots, at some steady state. Grid resolution is 512^2 and Ekman friction $\alpha = -1$.

where $\boldsymbol{x}_i(t)$ is the position of the ith tracer particle and $\boldsymbol{u}(\boldsymbol{x}_i(t), t)$ is the Eulerian velocity field projected at $\boldsymbol{x}_i(t)$. Figure 1 shows the snapshot of tracer particles distributed in a steady-state turbulent vorticity field. In what follows, we present a systematic report of our observations on tracer transport and derive its scaling with Ekman friction.

III. OBSERVATIONS AND DISCUSSIONS

A. Crossover time

We first compute the mean square displacement (MSD) of the tracer particles as

$$\langle \Delta \boldsymbol{x}^2 \rangle = \left\langle \frac{1}{N} \sum_{i=1}^{N} |\boldsymbol{x}_i(t) - \boldsymbol{x}_i(0)|^2 \right\rangle, \tag{4}$$

where $\langle \cdot \rangle$ denotes an ensemble average over 75 independent initial conditions. As is evident from Fig. 2, there is a ballistic regime at $t \ll \tau_c$, where due to correlations in velocity field, we observe $\langle \Delta \boldsymbol{x}^2 \rangle \sim t^2$. At late times, i.e., $t \gg \tau_c$, we observe a diffusive regime where $\langle \Delta \boldsymbol{x}^2 \rangle \sim t$, due to loss of memory. The crossover from ballistic to diffusive regime happens at an intermediate timescale τ_c that essentially denotes the relaxation time of the passive tracers. Interestingly, we observe that τ_c develops a minimum at $\alpha = 0$, directly implying that the fastest relaxation occurs at zero friction (see Fig. 2 inset). To understand this nonmonotonic behavior, we propose to identify $\tau_c \sim \ell^*/u_{\rm rms}$ where the length scale $\ell^* = 1/k^*$ with k^* being the location of the peak of the energy spectrum (refer to Fig. 3) and the velocity scale $u_{\rm rms} = \sqrt{\langle |\boldsymbol{u}|^2 \rangle}$ in the steady state. In Fig. 4 we show that both these timescales are in close agreement and display a minimum at $\alpha = 0$, clearly justifying our choice. A physical reasoning for this observed minimum can be constructed by noticing that $1/|\alpha|$ is a timescale over which advective terms necessary to develop turbulence, are damped ($\alpha > 0$) or accelerated ($\alpha < 0$). If we further realize that l_0/u_0 is a timescale over which the unstable modes grow due to stress-induced instabilities, the necessary condition for developed turbulence can be constructed through a ratio (refer to the Supporting Information of [17])

$$\mathcal{R} \sim \frac{u_0}{l_0|\alpha|} \sim \frac{\Gamma_0^2}{\Gamma_2|\alpha|} \gg 1. \tag{5}$$

We see that for $\alpha \to 0$, the above inequality is automatically established for arbitrary values of the parameters $\Gamma_{0,2}$. Since the transport of tracers is aided by background turbulence, the crossover

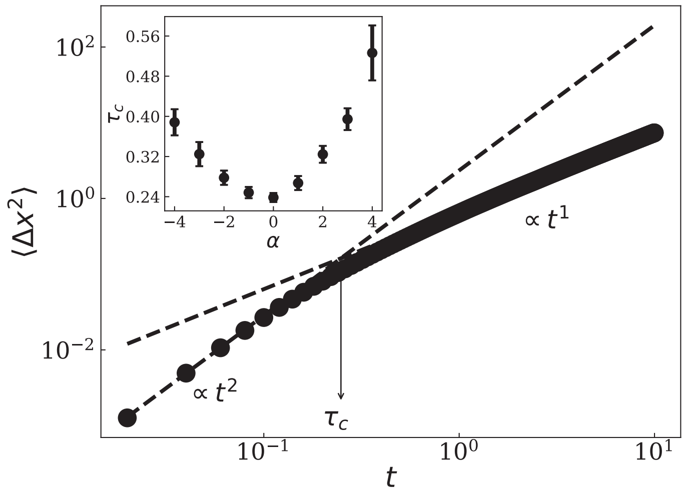

FIG. 2. Mean-square displacement $\langle \Delta \boldsymbol{x}^2 \rangle$ vs time t for a typical Ekman friction α. Inset: Crossover time τ_c develops a minimum at zero friction (see text for details). Error bars indicate one standard deviation.

from ballistic to diffusive regime must be fastest at zero friction. One can also understand the nonmonotonic behavior of τ_c by examining the velocity autocorrelation of tracers. It is evident from Fig. 5 that the case $\alpha \neq 0$ has the effect of leaving the Lagrangian velocities correlated over longer times. Below the value zero, as α becomes more negative, the velocity of the bacteria is increasingly propelled, thereby delaying the relaxation time of Lagrangian velocities. Similarly, above the value zero, as α becomes more positive, the velocity of the bacteria is increasingly damped, again leading to delayed relaxation of the Lagrangian velocities. Put simply, the effect of $\alpha \neq 0$ is to delay the loss of memory. In what follows, we provide scaling laws for both ℓ^* and u_{rms} that is further used to set up a friction scaling law for diffusion coefficient $\mathcal{D}$ in our active fluid.

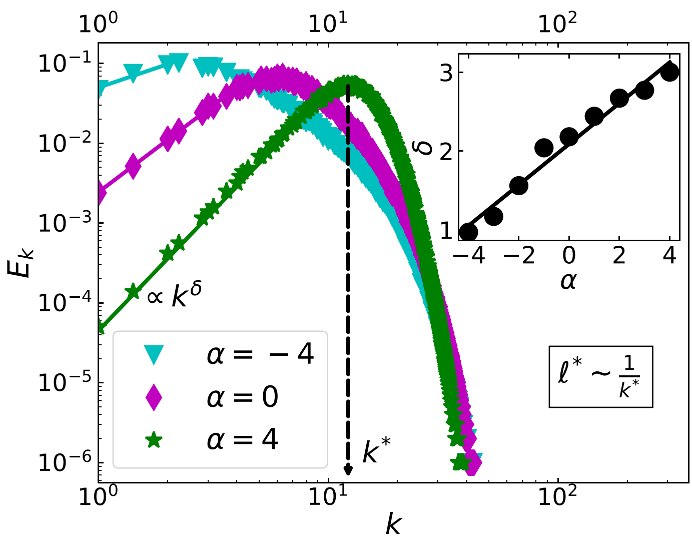

FIG. 3. Energy spectrum E_k for different values of Ekman friction α. The peak shows the location of dominant length scale $k^* = 1/\ell^*$. Inset: The exponent δ at low wave numbers is seen to be linear in α.

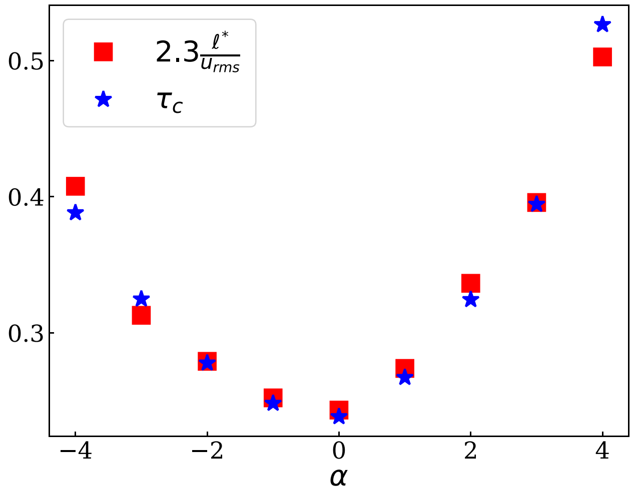

FIG. 4. Crossover time τ_c and the scale combination $\ell^*/u_{\rm rms}$. The prefactor turns out to be 2.3 for the best fit.

B. Scaling laws for ℓ^* and $u_{\rm rms}$

Recently, an expression for the energy spectrum of our model fluid was derived in Ref. [19] as

$$E_k = E_0 k^{\delta} \exp(-E_1 k^2), \tag{6}$$

where the constants $E_{0,1}$ depend on model parameters excluding α. The location of the peak $k^* \sim 1/\ell^*$ can be easily obtained by extremizing Eq. (6), yielding

$$k^* \sim \sqrt{\delta}, \tag{7}$$

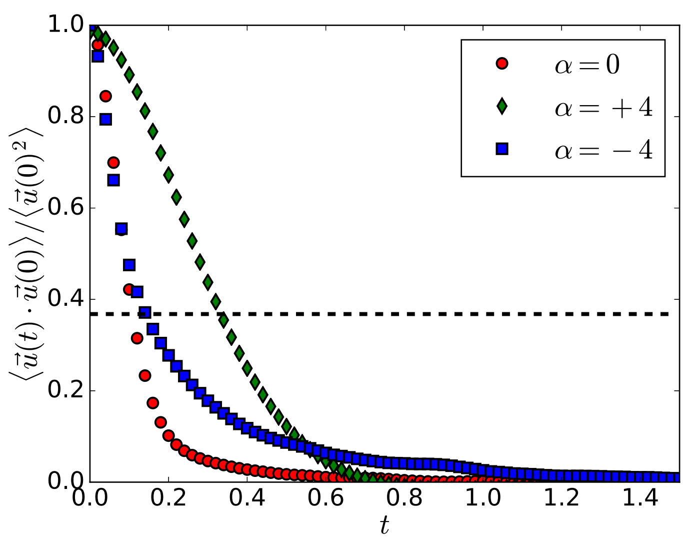

FIG. 5. Velocity autocorrelation of tracers for different values of Ekman friction α. It is evident that the relaxation (e-folding) time is fastest for the case $\alpha = 0$ and becomes progressively higher for both self-propulsion ($\alpha < 0$) and damping ($\alpha > 0$).

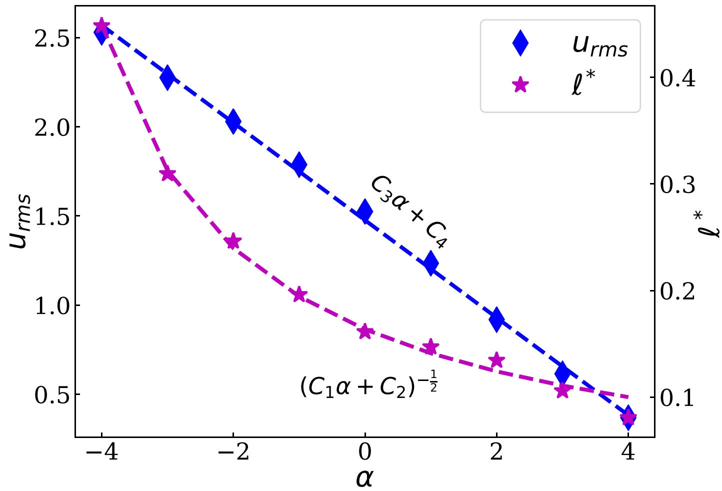

FIG. 6. Characteristic length (ℓ^*) and velocity (u_{rms}) scales along with their predicted scalings shown as dashed lines.

which together with the observation that δ is linear in α (see Fig. 3) leads us to the following scaling:

$$\ell^* \sim (C_1\alpha + C_2)^{-1/2}, \tag{8}$$

where the constants $C_{1,2}$ are the fitting parameters which will depend on other variables of the governing model. The linear relationship between δ and α was already established in [19] for the range $\alpha \in [-1, 4]$. In our study we have explicitly observed that the relationship holds well even for the wide regime of interest $\alpha \in [-4, 4]$.

Next we derive the scaling for u_{rms} by focusing on the kinetic energy of the fluid in the steady state. To that end, we rewrite Eq. (1) as

$$\frac{\partial \boldsymbol{u}}{\partial t} + \lambda_0\left[\frac{1}{2}\nabla(\boldsymbol{u}\cdot\boldsymbol{u}) - \boldsymbol{u}\times\boldsymbol{\omega}\right] = -\nabla P + \Gamma_0\nabla\times\boldsymbol{\omega} - \Gamma_2\nabla\times\nabla\times\nabla\times\boldsymbol{\omega} - \alpha\boldsymbol{u} - \beta|\boldsymbol{u}|^2\boldsymbol{u}, \tag{9}$$

and by taking a scalar product of $\boldsymbol{u}$ with Eq. (9) we arrive at the energy equation

$$\begin{aligned}\frac{\partial}{\partial t}\frac{|\boldsymbol{u}|^2}{2} + \frac{\lambda_0}{2}\nabla\cdot(|\boldsymbol{u}|^2\boldsymbol{u}) = -\nabla\cdot(P\boldsymbol{u}) - \Gamma_0[\nabla\cdot(\boldsymbol{u}\times\boldsymbol{\omega}) - |\boldsymbol{\omega}|^2] - \Gamma_2\{\nabla\cdot[(\nabla\times\nabla\times\boldsymbol{\omega})\times\boldsymbol{u}]\\ - (\nabla^2\boldsymbol{\omega})\cdot\boldsymbol{\omega}\} - \alpha|\boldsymbol{u}|^2 - \beta|\boldsymbol{u}|^4.\end{aligned} \tag{10}$$

The approximation of statistical homogeneity and spatial isotropy allows us to perform a spatial (ensemble) average of the above equation and put all divergences to zero, leading us to

$$\frac{d}{dt}\frac{\langle|\boldsymbol{u}|^2\rangle}{2} = \Gamma_0\langle\boldsymbol{\omega}^2\rangle + \Gamma_2\langle(\nabla^2\boldsymbol{\omega})\cdot\boldsymbol{\omega}\rangle - \alpha\langle|\boldsymbol{u}|^2\rangle - \beta\langle|\boldsymbol{u}|^4\rangle. \tag{11}$$

Further, under conditions of steady state we drop the time derivative, and by using the scaling

$$\begin{aligned}\langle\omega^2\rangle &\sim u_{\mathrm{rms}}^2/\ell^{*2},\\ \langle(\nabla^2\boldsymbol{\omega})\cdot\boldsymbol{\omega}\rangle &\sim u_{\mathrm{rms}}^2/\ell^{*4}\end{aligned} \tag{12}$$

in Eq. (11), we are led to

$$0 \approx \Gamma_0 u_{\mathrm{rms}}^2/\ell^{*2} + \Gamma_2 u_{\mathrm{rms}}^2/\ell^{*4} - \alpha u_{\mathrm{rms}}^2 - \beta u_{\mathrm{rms}}^4, \tag{13}$$

which together with the scaling for ℓ^* [refer to Eq. (8)], yields

$$u_{\rm rms} \sim C_3\alpha + C_4, \tag{14}$$

where the constants $C_{3,4}$ again depend on other parameters of the governing model. In Fig. 6, we present a direct comparison of these scalings [Eqs. (8) and (14)] with the numerically extracted values of $\ell^* = 1/k^*$ and $u_{\rm rms} = \sqrt{\langle |\boldsymbol{u}|^2\rangle}$ and observe an excellent agreement between them. To assert the quality of our prediction, we will now present a scaling law for the tracer diffusion coefficient that remains valid throughout the range of Ekman friction explored in our work.

C. Scaling law for diffusion coefficient ($\mathcal{D}$)

Denoting the Lagrangian velocity of the ith tracer $\boldsymbol{u}(\boldsymbol{x}_i(t), t) = \boldsymbol{u}_i(t)$, we take the time derivative of the squared displacement of the ith tracer as

$$\frac{d}{dt}\Delta\boldsymbol{x}_i^2 = 2\Delta\boldsymbol{x}_i \cdot \boldsymbol{u}_i(t) = 2\boldsymbol{u}_i(t)\cdot\int_0^t \boldsymbol{u}_i(t')dt', \tag{15}$$

which under the change of variable $\tau = t - t'$ yields

$$\frac{d}{dt}\Delta\boldsymbol{x}_i^2 = 2\int_0^t \boldsymbol{u}_i(t)\cdot\boldsymbol{u}_i(t-\tau)d\tau. \tag{16}$$

Averaging over all particles as well as the ensemble yields

$$\frac{d}{dt}\langle\Delta\boldsymbol{x}^2\rangle = \frac{2}{N}\int_0^t \left\langle \sum_{i=1}^N \boldsymbol{u}_i(t)\cdot\boldsymbol{u}_i(t-\tau)\right\rangle d\tau, \tag{17}$$

which in the diffusive regime ($t \gg \tau_c$) reduces to

$$\frac{d}{dt}\langle\Delta\boldsymbol{x}^2\rangle \approx 2u_{\rm rms}^2\tau_c \approx 2u_{\rm rms}\ell^*, \tag{18}$$

where the last approximation follows from our proposed scaling relation $\tau_c \approx \ell^*/u_{\rm rms}$. Using Einstein's formula (in 2D) $\langle\Delta\boldsymbol{x}^2\rangle = 4\mathcal{D}t$, Eq. (18) becomes

$$\mathcal{D} \approx u_{\rm rms}\ell^*/2. \tag{19}$$

Further using the scalings for ℓ^* and $u_{\rm rms}$ respectively from Eqs. (8) and (14), we are led to a simple scaling formula

$$\mathcal{D} \sim (C_3\alpha + C_4)/\sqrt{C_1\alpha + C_2}. \tag{20}$$

The beauty of this simple scaling law is immediately evident in Fig. 7 where we show an excellent agreement with the diffusion coefficient directly extracted from the MSD data and the characteristic scales, ℓ^* and $u_{\rm rms}$. Quite interestingly, the scaling law remains valid over a wide range of friction, i.e., $\alpha \in [-4, 4]$ clearly indicating the robustness of our results. To demonstrate generality, we have verified that our scaling laws hold over variations in other free parameters of the model, say β (see Fig. 7). In the following, we provide a realization of a typical 2D experimental setup where our predictions are of good utility.

IV. EXPERIMENTAL REALIZATION

Modern particle tracking methods have come a long way in understanding transport in quasi-two-dimensional bacterial suspensions [27,28]. It is also possible to conduct an experimental study that will help in the physical realization of our theoretical predictions, and below we provide a detailed comparison of the numerical parameters in the simulation with physical quantities in real units. To remain consistent, the numerical values for the physical parameters are taken in the same range as reported in Ref. [17].

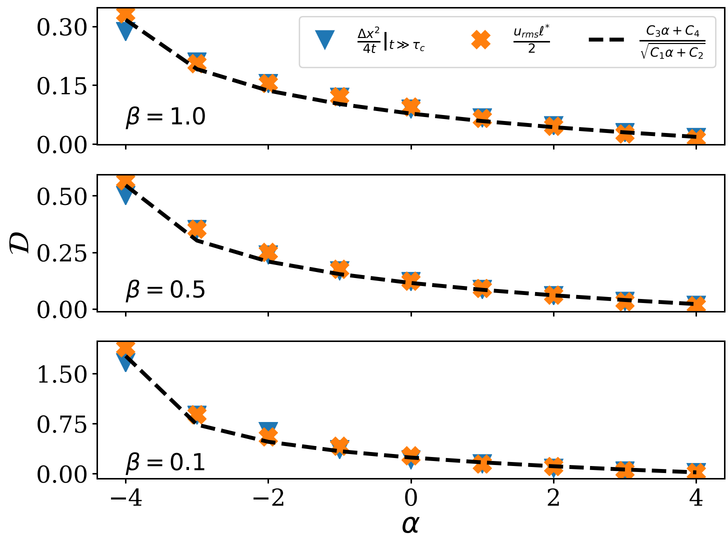

FIG. 7. Diffusion coefficient $\mathcal{D}$ vs Ekman friction α for different values of the free parameter β. Both the estimates of $\mathcal{D}$, namely, from the simulations $\langle \Delta \boldsymbol{x}^2 \rangle / 4t$, and from characteristic scales $u_{\text{rms}} \ell^* / 2$, agree very well with our predicted scaling law [Eq. (20), dashed line]. The figure shows the generality of our scaling law as it holds over variation in the free parameters of our governing model, in this case β.

The characteristic unit l_0 can be obtained by choosing an experimental viewing area that contains roughly the same number of vortices as our 2D simulation box. For example, a correspondence of 4×10^4 μm^2 viewing area with our simulation box directly corresponds to $l_0 \approx 32$ μm in physical units. Next, u_0 can be taken to be of the order of typical bacterium swimming speeds, say 25 μm/s. Fixing these values of u_0 and l_0, we can write $\Gamma_0 \approx 36$ μm^2/s and $\Gamma_2 \approx 75$ μm^4/s. Finally we can write our time unit $t_0 = l_0/u_0 \approx 1.3$ s. The parameter β used in the continuum model is given a small positive value from stability constraints, to enforce a normal distribution on the fluid velocities that is typically seen in experiments. We fix $\beta = 0.5$ (reduced units) in all our simulations to remain consistent with the earlier works on this continuum model. The polar velocity ($\alpha < 0$) of the bacterium $u_P = \sqrt{|\alpha|/\beta}$ which positively correlates with the available nutrient/oxygen concentration can be directly extracted from the experiments [7]. In table I, we list some possible values of the Ekman friction α readily obtained in various polar ordered phases. Our choices of $|\alpha|$ correspond to the typical polar swimming speed of bacteria that can vary up to a few hundred micrometers per second [17,20,29]. The regime of $\alpha > 0$ corresponds to isotropic disordered state, where bacteria will not have global polar alignment. In such situations, α can be merely inferred as a linear drag associated with any fluid motion that arises due to the interaction between the bacterial units and their environment. We conclude our paper below by summarizing the observations and results.

TABLE I. Ekman friction $\alpha < 0$ for various ordered phases.

u_P/u_0 ($u_0 = 25$ μm/s)	$\lvert\alpha\rvert t_0$ ($t_0 = 1.3$ s)	$\lvert\alpha\rvert$ (in physical units, s^{-1})
1.0	0.5	0.4
1.5	1.1	0.8
2.0	2.0	1.5

V. CONCLUSION

We have investigated in detail the problem of turbulent transport of passive (Lagrangian) tracers in a model active fluid that well describes dense bacterial suspensions. We show that in the fully developed turbulence, the tracer transport exhibits a crossover from ballistic to diffusive regime at a timescale τ_c that attains a minimum at zero friction. We explain this observation by measuring a characteristic length scale ℓ^* extracted from the energy spectrum peak and a characteristic velocity scale u_{rms} extracted from the total kinetic energy in the steady state. Further, by assuming statistical homogeneity and isotropy in the steady state we are able to provide scaling laws for both ℓ^* and u_{rms} that hold well over a wide range of Ekman friction, namely, from the regime of strong energy damping to the regime of strong energy injection. Finally, we use these characteristic scales to develop a friction scaling law for the late time diffusion coefficient $\mathcal{D}$. It is worth mentioning here that the dependence of $\mathcal{D}$ on α in our work qualitatively agrees with the observation of enhanced diffusion in Refs. [30,31]. Further, the beauty of this scaling law lies in the fact that the transport coefficient is predicted from the characteristics of the governing model and the knowledge of the energy spectrum. The reported laws are universal and are not affected by changes in the other parameters (see Fig. 7) of the governing model and should apply well to any generic fluid not limited to bacterial suspensions alone. We believe that our work, which uses a simple continuum model with minimum number of free parameters, should contribute to the knowledge in the field of active turbulence and transport in active fluids. The findings of our work should also draw the attention of fluid dynamics researchers who are interested in pursuing the statistical laws that remain universal over general patterns of energy injection and dissipation.

ACKNOWLEDGMENTS

We thank Abhijit Sen and Gautam Menon for discussions and comments on the manuscript. All simulations were done on the VIRGO super cluster of IIT Madras. Support from DST INSPIRE Faculty Grant 2013/PH-59 is gratefully acknowledged.

---

[1] U. Frisch, *Turbulence: The Legacy of A.N. Kolmogorov* (Cambridge University Press, Cambridge, UK, 1995).

[2] P. Davidson, *Turbulence: An Introduction for Scientists and Engineers* (Oxford University Press, New York, 2015).

[3] R. H. Kraichnan, Inertial ranges in two-dimensional turbulence, Phys. Fluids **10**, 1417 (1967).

[4] G. Boffetta and R. E. Ecke, Two-dimensional turbulence, Annu. Rev. Fluid Mech. **44**, 427 (2012).

[5] J. O. Kessler, Collective behavior and dynamics of swimming bacteria, *Bacteria as Multicellular Organisms* (Oxford University Press, New York, 1997).

[6] A. Sokolov, I. S. Aranson, J. O. Kessler, and R. E. Goldstein, Concentration Dependence of the Collective Dynamics of Swimming Bacteria, Phys. Rev. Lett. **98**, 158102 (2007).

[7] A. Sokolov and I. S. Aranson, Physical Properties of Collective Motion in Suspensions of Bacteria, Phys. Rev. Lett. **109**, 248109 (2012).

[8] C. Dombrowski, L. Cisneros, S. Chatkaew, R. E. Goldstein, and J. O. Kessler, Self-Concentration and Large-Scale Coherence in Bacterial Dynamics, Phys. Rev. Lett. **93**, 098103 (2004).

[9] D. L. Koch and G. Subramanian, Collective hydrodynamics of swimming microorganisms: Living fluids, Annu. Rev. Fluid Mech. **43**, 637 (2011).

[10] S. P. Thampi, R. Golestanian, and J. M. Yeomans, Velocity Correlations in an Active Nematic, Phys. Rev. Lett. **111**, 118101 (2013).

[11] S. Ramaswamy, The mechanics and statistics of active matter, Annu. Rev. Condens. Matter Phys. **1**, 323 (2010).

[12] A. Baskaran and M. C. Marchetti, Statistical mechanics and hydrodynamics of bacterial suspensions, Proc. Natl. Acad. Sci. USA **106**, 15567 (2009).
[13] K. Kruse, J.-F. Joanny, F. Jülicher, J. Prost, and K. Sekimoto, Asters, Vortices, and Rotating Spirals in Active Gels of Polar Filaments, Phys. Rev. Lett. **92**, 078101 (2004).
[14] D. Saintillan and M. J. Shelley, Instabilities, pattern formation, and mixing in active suspensions, Phys. Fluids **20**, 123304 (2008).
[15] R. A. Simha and S. Ramaswamy, Hydrodynamic Fluctuations and Instabilities in Ordered Suspensions of Self-Propelled Particles, Phys. Rev. Lett. **89**, 058101 (2002).
[16] M. C. Marchetti, J. F. Joanny, S. Ramaswamy, T. B. Liverpool, J. Prost, M. Rao, and R. A. Simha, Hydrodynamics of soft active matter, Rev. Mod. Phys. **85**, 1143 (2013).
[17] H. H. Wensink, J. Dunkel, S. Heidenreich, K. Drescher, R. E. Goldstein, H. Löwen, and J. M. Yeomans, Meso-scale turbulence in living fluids, Proc. Natl. Acad. Sci. USA **109**, 14308 (2012).
[18] J. Dunkel, S. Heidenreich, M. Bär, and R. E. Goldstein, Minimal continuum theories of structure formation in dense active fluids, New J. Phys. **15**, 045016 (2013).
[19] V. Bratanov, F. Jenko, and E. Frey, New class of turbulence in active fluids, Proc. Natl. Acad. Sci. USA **112**, 15048 (2015).
[20] J. Dunkel, S. Heidenreich, K. Drescher, H. H. Wensink, M. Bär, and R. E. Goldstein, Fluid Dynamics of Bacterial Turbulence, Phys. Rev. Lett. **110**, 228102 (2013).
[21] M. James and M. Wilczek, Vortex dynamics and Lagrangian statistics in a model for active turbulence, Eur. Phys. J. E **41**, 21 (2018).
[22] M. James, W. J. T. Bos, and M. Wilczek, Turbulence and turbulent pattern formation in a minimal model for active fluids, Phys. Rev. Fluids **3**, 061101 (2018).
[23] J. Swift and P. C. Hohenberg, Hydrodynamic fluctuations at the convective instability, Phys. Rev. A **15**, 319 (1977).
[24] J. Toner, Y. Tu, and S. Ramaswamy, Hydrodynamics and phases of flocks, Ann. Phys. (NY) **318**, 170 (2005).
[25] J. Toner and Y. Tu, Flocks, herds, and schools: A quantitative theory of flocking, Phys. Rev. E **58**, 4828 (1998).
[26] C. Canuto, M. Y. Hussaini, A. Quarteroni, and A. Thomas, Jr., *Spectral Methods in Fluid Dynamics* (Springer Science & Business Media, Berlin, 2012).
[27] Xiao-Lun Wu and Albert Libchaber, Particle Diffusion in a Quasi-Two-Dimensional Bacterial Bath, Phys. Rev. Lett. **84**, 3017 (2000).
[28] Y. Peng, L. Lai, Y.-S. Tai, K. Zhang, X. Xu, and X. Cheng, Diffusion of Ellipsoids in Bacterial Suspensions, Phys. Rev. Lett. **116**, 068303 (2016).
[29] T. Ishikawa, Suspension biomechanics of swimming microbes, J. R. Soc., Interface **6**, 815 (2009).
[30] A. Morozov and D. Marenduzzo, Enhanced diffusion of tracer particles in dilute bacterial suspensions, Soft Matter **10**, 2748 (2014).
[31] G. Mino, T. E Mallouk, T. Darnige, M. Hoyos, J. Dauchet, J. Dunstan, R. Soto, Y. Wang, A. Rousselet, and E. Clement, Enhanced Diffusion Due to Active Swimmers at a Solid Surface, Phys. Rev. Lett. **106**, 048102 (2011).